International Journal of Hydrogen Energy 87 (2024) 917–927

Contents lists available at ScienceDirect

International Journal of Hydrogen Energy

journal homepage: www.elsevier.com/locate/he

A phenomenological hydrogen induced edge dislocation mobility law for bcc Fe obtained by molecular dynamics

Mehmet Furkan Baltacioglu [a], Mehmet Fazil Kapci [a], J. Christian Schön [b], Jaime Marian [c], Burak Bal [a,*]

[a] Department of Mechanical Engineering, Abdullah Gül University, 38080 Kayseri, Turkiye
[b] Max Planck Institute for Solid State Research, Heisenbergstr. 1, 70569, Stuttgart, Germany
[c] University of California, 400 Westwood Plaza, Los Angeles, CA, 90095, USA

ARTICLE INFO

Handling Editor: Dr S Nanda

Keywords:
Hydrogen embrittlement
Molecular dynamics
Dislocation
Mobility law
HELP mechanism

ABSTRACT

Investigating the interaction between hydrogen and dislocations is essential for understanding the origin of hydrogen-related fractures, specifically hydrogen embrittlement (HE). This study investigates the effect of hydrogen on the mobility of ½<111>{110} and ½<111>{112} edge dislocations in body-centered cubic (BCC) iron (Fe). Specifically, molecular dynamics (MD) simulations are conducted at various stress levels and temperatures for hydrogen-free and hydrogen-containing lattices. The results show that hydrogen significantly reduces dislocation velocities due to the pinning effect. Based on the results of MD simulations, phenomenological mobility laws for both types of dislocations as a function of stress, temperature and hydrogen concentration are proposed. Current findings provide a comprehensive model for predicting dislocation behavior in hydrogen-containing BCC lattices, thus enhancing the understanding of HE. Additionally, the mobility laws can be utilized in dislocation dynamics simulations to investigate hydrogen-dislocation interactions on a larger scale, aiding in the design of HE-resilient materials for industrial applications.

1. Introduction

Hydrogen embrittlement (HE) is a phenomenon where the presence of hydrogen in metallic materials leads to unexpected failures [1]. HE remains a persistent issue affecting a wide range of industrial applications, ranging from cars, aviation, oil & gas storage and transportation systems, to high-strength materials for infrastructure applications [2–8]. The reason is that HE leads to a deterioration of the mechanical properties of metals, both during their manufacturing and while in use [9,10]. From a variety of sources in the environment, and due to the easy absorption of hydrogen into the crystal lattice of most metals, the prevention of HE constitutes a great challenge to the materials scientist and engineer [11]. It is well-known that the degree of HE is sensitive to a variety of mechanical, environmental and material related factors [9,12–14], with sometimes rather complex outcomes and dependencies. For instance, when decreasing the strain rate one would expect that the effect of foreign atoms like hydrogen on the properties of the material should be weaker, but such a decrease also allows more time for hydrogen-dislocation interactions to take place, and thus often increases the effective susceptibility of the material to HE [15–17]. In addition, the susceptibility of HE usually grows with the mechanical strength of a material, often in a roughly linearly fashion [18]. The effect of these 3 main factors, material, mechanical, environmental on the HE susceptibility of different materials is well-studied [9,12,19]. However, these studies mostly focus on the changes in the mechanical properties on a macroscopic level. In order to better understand the underlying atomic and mesoscopic mechanisms of HE, it is necessary to work on different time and length scales.

There are various experimental and numerical studies in literature that aim to understand the nature of HE at the atomic scale, and as a result of these studies, different mechanisms of HE have been proposed [12,20]. Among these mechanisms, hydrogen enhanced localized plasticity (HELP) and hydrogen enhanced decohesion (HEDE) have become the most widely accepted HE mechanisms by the researchers [16,21–25]. HELP states that hydrogen shields the elastic stress field of dislocations and thus increases the mobility of dislocations and cause localized plasticity [12,26]. In contrast, HEDE suggests that hydrogen within the lattice reduces the cohesive strength of the metal-metal and

* Corresponding author.
E-mail address: burak.bal@agu.edu.tr (B. Bal).

https://doi.org/10.1016/j.ijhydene.2024.08.509
Received 12 June 2024; Received in revised form 27 August 2024; Accepted 31 August 2024
Available online 11 September 2024

therefore promotes crack growth finally resulting in mechanical [12]. For many years, the formation mechanism of HE has been debated, and it has generally been assumed that intergranular fracture in systems that do not form hydrides is due to HEDE [12,27]. However, based on subsequent experimental observations, it has been argued that dislocation plasticity and, therefore, HELP plays a much more significant role as an HE mechanism [28]. In the last decade, it has been demonstrated that both of these mechanisms can be activated individually or simultaneously under different conditions [16,21–25]. Despite these extensive studies, the exact mechanism of HE still remains unclear [29]. Thus, to understand the nature of HE, interactions between hydrogen and dislocations at both atomic and mesoscopic scales need to be further analyzed, ideally on the quantum mechanical level.

Employing ab initio simulations performed at the atomic level, various problems have been investigated in the past, such as the segregation of hydrogen to interfacial regions [30], hydrogen-vacancy interactions [31], diffusion of hydrogen in different metal phases [32], and the thermodynamics of hydrogen solubility [33]. However, due to the limited number of atoms that can be studied on the ab initio level, dislocation-hydrogen interactions cannot be observed on relevant time scales, and thus this type of modelling is limited in its explanatory power regarding the atomic mechanisms underlying HE. Molecular dynamics (MD) studies using empirical, semi-empirical or effective potentials have been conducted to examine the atomic origin of HE. These include the investigation of processes such as hydrogen diffusion and localization within the lattice, and of the effects of hydrogen on macroscopic mechanical properties, microstructure, surface energy and dislocation velocity [20]. From various studies, also showing controversial results, it was observed that presence of hydrogen decreased the velocity of edge dislocations; however, once the dislocation speed is decreased hydrogen can also enhance the dislocation's velocity and promote the HELP mechanism [20,34,35]. Similarly, a high hydrogen concentration impedes kink-pair nucleation and migration and decreases the velocity of a screw dislocation, while a low concentration of hydrogen promotes kink-pair nucleation and migration and therefore enhances the mobility of screw dislocations [36]. However, to the best of the authors' knowledge, no study reveals the effect of hydrogen on the mobility laws of dislocations. Since the dislocation mobility plays a crucial role in dictating various aspects of plastic deformation, knowing the precise impact of hydrogen on dislocation mobility is of utmost significance in comprehending the nature of HE [20].

Slip takes place within face-centered cubic (FCC) metals on close-packed {111} planes and <110> directions [37]. Low lattice resistance of FCC and planar core structure of edge dislocation results in dislocation glide being regulated solely by the applied shear stress [38]. This suggests that, the mobility laws for FCC systems should adhere to Schmid's law [38]. In contrast, dislocations experience a great amount of lattice resistance in body centered cubic (BCC) metals [38]. In BCC metals, slip mostly occurs on {110} and {112} planes and <111> directions [37]. When the dislocation velocity is much smaller than the shear wave speed, interaction of phonons with dislocations is the dominant activation mechanism of edge dislocations [39]. Therefore, in BCC crystal systems edge dislocations still move very rapidly via phonon drag, and thermally activated motion of screw dislocations dominates the plastic deformation [38,39]. In the literature, ½<111>{110} and ½<111>{112} edge dislocation mobility laws in BCC systems have been studied [39–41] and phenomenological dislocation mobility laws for BCC have been proposed for both edge and screw dislocations [38]. In these studies, three main effects were observed: 1) The mobility laws assume that the velocity of dislocation is linearly proportional to the applied stress [38]. In the supersonic region, the dislocation velocity becomes equal to the speed of sound, as relativistic effects and dissipation mechanisms are neglected [38], 2) The drag coefficient of the mobility laws depends only on the type of dislocation and the temperature [38,39]. Finally, 3) the motion of the ½<111>{110} type of edge dislocation is very fast, and the nucleation of kinks is a-thermal [39]. Therefore, this type does not contribute to plastic flow to any large degree [39]. On the other hand, ½<111>{112} dislocations exhibit both phonon drag and thermally activated regimes, and thus contribute noticeably to the plasticity of materials [39]. As a consequence, screw dislocations are the dominant dislocation type for plastic flow [39]. However, when hydrogen diffuses into the lattice, it tends to concentrate around edge dislocations and decrease their elastic energy [42]. This might make the system more likely to promote plastic deformations over screw dislocations [42]. To clarify this issue and in order to understand the atomic origin of HE in BCC structures, MD simulations of hydrogen-free and hydrogen-containing lattices are needed. Furthermore, the effect of hydrogen on the drag has to be analyzed, such that the laws that govern the corresponding hydrogen enhanced mobility can be developed. Up to now, there is only one study in literature addressing this issue [43]. In that study, hydrogen enhanced mobility law of screw dislocation has been proposed [43]. However, that investigation did not involve any MD simulations; instead Kinetic Monte Carlo (KMC) simulation were performed and only screw dislocations were studied. To our knowledge, there is currently no existing literature that explores the mobility law of edge dislocations under the influence of hydrogen.

In the present study, the effects of hydrogen on the mobility laws of edge dislocations have been investigated for ½<111>{110} and ½<111>{112} dislocations in α-Fe. For this purpose, MD simulations of length 1 ns were conducted for lattices both without and with hydrogen. The simulations for ½<111>{110} dislocations were carried out using 4 different hydrogen concentrations (%0 H/Fe, %0.1 H/Fe, %0.25 H/Fe and %0.5 H/Fe) and 5 different temperatures (50 K, 100 K, 200 K, 300 K and 400 K); in addition, for pure iron (%0 H/Fe), simulations at a temperature of 500 K were performed. On the other hand, the simulations for ½<111>{112} dislocations were conducted at 5 different temperature values (100 K, 200 K, 300 K, 400 K and 500 K) for (%0 H/Fe, %0.1 H/Fe, %0.25 H/Fe and %0.5 H/Fe) hydrogen concentration values. The effect of hydrogen on the measured stress and displacement as function of time and velocity-stress relationship for both hydrogen-free and hydrogen-containing lattices have been investigated. It was observed that hydrogen impeded the movement of dislocations. Furthermore, a formula for the effect of hydrogen on the drag coefficient has been developed, and corresponding closed-form laws for the hydrogen enhanced mobility have been obtained. These mobility laws then can be used for discrete dislocation dynamics simulation in order to investigate hydrogen-dislocation interactions at micro scale.

2. Method

The MD simulations were performed using the LAMMPS (Large-scale Atomic/Molecular Massively Parallel Simulator) code. The simulations employed the embedded atom method (EAM) potential presented by M. Wen [44]. The potential effectively defines the interatomic potentials of H–H and Fe–H in the α-Fe structure, encompassing H-dislocation interactions and other defects [44]. This potential yields more reliable results than the Mendelev potential [45] for the simulation of hydrogen rich cells since it captures the repulsive effect of H–H interactions below 0.45 Å, that cannot be accounted for by the Mendelev potential. The hydrogen concentrations were selected as %0 H/Fe, %0.1 H/Fe, %0.25 H/Fe, and %0.5 H/Fe and the effects of the hydrogen concentration on the mobility of ½<111>{110} and ½<111>{112} edge dislocations were investigated under shear loading. The cell dimensions were specified as 29.6 nm × 20.2 nm × 28.3 nm. These dimensions were chosen for the following reasons: 1) The X-axis was long enough to allow activation of the kink-nucleation mechanisms, 2) the length of the Y-axis was chosen to minimize the image forces along the glide plane, 3) the length of the Z-axis was chosen to ensure the distribution of mechanical work done during dislocation slip, indirect heat production without the periodic boundary conditions being met, and 4) to be compatible with the literature [39] as far as similar calculations have been performed. Within this simulation cell, about 1.5 million Fe atoms were employed

for the pure case (%0 H/Fe). All simulations were conducted using PPS (Periodic-Periodic-Shrink) boundary conditions in the x, y, and z axes. Along the x and y axes, periodic boundary conditions were applied to facilitate dislocation motion, while along the z-axis, a shrink-wrapped boundary condition was employed to maintain atoms at their specified positions. The simulations were conducted using the NVE (number of atoms, volume, and energy constant) ensemble and Langevin thermostat was employed to control the temperature within the region delineated by two layers in Fig. 1. In particular, whole MD simulation consists of many short pieces of NVE-type parts, between these one periodically adjusts both the volume and temperature, in order to keep the pressure and temperature at or close to the prescribed values. The configuration efficiently conserved enthalpy during the simulation, as given by $H = E + pV$. Fig. 1 illustrates the x, y, z axes, the initial position of the dislocation, the glide plane, the fixed atom layer, and the volume where the shear force was applied. In this configuration, hydrogen atoms were initially randomly placed but only up to a certain distance (7,1 nm) to the endpoints along the z-axis, in order to prevent hydrogen accumulation in these regions. Supplementary Figs. 1 and 2 illustrate the effect of relaxation time on hydrogen distribution. The results indicate that longer waiting does not alter the hydrogen distribution, with a random distribution of hydrogen atoms consistently observed. Supplementary Figures 3 through 16 illustrate that the distribution of hydrogen, both before and after relaxation, does not concentrate at the dislocation core and remains random at various hydrogen concentrations and temperatures. Additionally, during the motion of dislocation, hydrogen distribution is random as indicated in Supplementary Fig 17 through 19. As far as the placement of the hydrogen atoms in the x and y directions was concerned, no restrictions were employed. Thus, the (x,y,z) coordinates of the hydrogen atoms could take on random values within the lengths of Lx, Ly, Lz/2, and the allowed region where hydrogen was added constitutes half of the total cell volume. Of course, during the subsequent simulations, the hydrogen atoms moved into the previously hydrogen empty region of the simulation cell. The simulation cells underwent minimization before load applications, with a defined output time step of 0.2 ps? The systems were minimized until reaching equilibration temperatures of 50 K, 100 K, 200 K, 300 K, 400 K, and 500 K for all simulations. As depicted in Fig. 1, the simulation cell comprises three distinct regions. The first one, presented in blue, is where shear stress was applied. The shear stress is applied in the x-axis direction. The black region represents the fixed atom layers. The glide plane is presented in green, and the dislocation exhibits motion on this plane in the x-direction and the edge dislocation takes place in y axis. All atoms in the uncolored regions are free to move in response to the shear stress. The dislocations have a planar core structure. The simulations were conducted for a duration of 1 ns with a timestep of 1 fs? This time step is widely reported in the literature [46–55]. Subsequent to the MD simulations, the systems were visualized using OVITO software [56], and the dislocation's mobility was analyzed using the Dislocation Extraction Algorithm (DXA) [57]. Moreover, atomic stress calculations were conducted via the virial stress theorem.

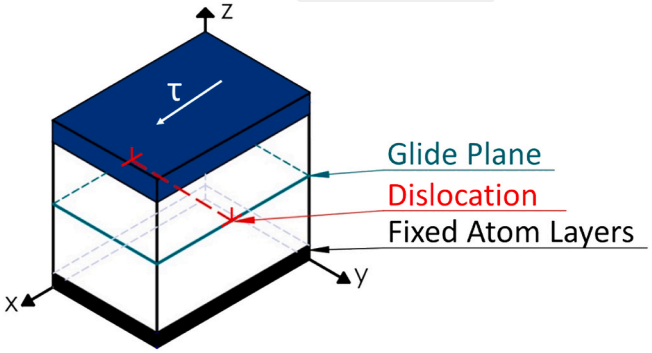

Fig. 1. Representative schematic of Simulation Cell. (unit: nm).

3. Results and discussion

3.1. Edge dislocation mobility on (110) plane

Fig. 2 displays stress vs. time graphs of simulations at 100 K temperature, encompassing pure iron, %0.1 H/Fe concentration, %0.25 H/Fe concentration, and %0.5 H/Fe concentration on (110) plane. All the simulations were conducted stress-controlled to minimize the stress fluctuations inside the simulation cell [58]. Additionally, stress-controlled simulations give dislocation velocities that are not bound to a specific strain rate, as the velocity calculations in these circumstances are unaffected by the size of the simulation box utilized. Notably, there is an increase in stress values until 0.5 ns? This increment is attributed to the fact that the stress was gradually raised from 0 MPa to the desired stress value during this period. Subsequently, between 0.5 ns and 1 ns, the stress values stabilize in comparison to the initial stages. The applied stress values from the upper part of the cell were higher than the corresponding graphic stress values, except for the stresses where dislocation motions could not be observed. Due to friction and the loss of energy caused by atom motion in the system, some of this stress value is consumed, resulting in a decrease in the observed stress values in the graphs. Another result is that periodic fluctuations in stress values in hydrogen-free simulations start at lower stress levels compared to those in hydrogen-containing simulations. The reason behind this is that we could not observe any sustained motion under fluctuating stress values, but just some vibration-like motion of the dislocation. Starting from fluctuated stresses, the dislocation starts its motion. After the motion becomes stable, the stress also becomes stable; hence, the region of lower stress shortly before stable dislocation movement was considered as the transition region. The result can be interpreted in the following way: if the stress value is just large enough for initiating the motion of the dislocation, stress fluctuations become dominant, but if the stress value is greater than this value, the stress fluctuations decrease and the movement of the dislocation becomes smooth. Moreover, due to the dislocation pinning effect of hydrogen [20], the transition occurs at greater stresses with the addition of hydrogen to pure iron and our results agree well with literature [59,60]. This clearly shows the effect of hydrogen on the system dynamics. Fig. 2 presents simulations at 100 K, while the results for other temperatures can be accessed in. Supplementary Figures 20 through 23

Fig. 3 shows the dislocation core displacement vs time graphs of the hydrogen free lattice at temperatures at 50 K, 100 K, 200 K, 300 K, 400 K and 500 K temperatures. It can be observed that increasing stress values resulted in greater displacement. It had been previously reported that the migration of an edge dislocation on (111) plane occurs without any kink formation and alteration of the core structure in the absence of hydrogen [61]. In addition, the motion of an edge dislocation is not thermally activated; instead, phonon drag is the main mechanism of the edge dislocation glide [39]. Therefore, dislocations could move at low stress values in the absence of hydrogen, and our results correspond well with previous studies in the literature [39]. At low applied stress values, the lattice resistance could affect the dislocation motion (Fig. 3d–f at 100 MPa) but at higher stress values the lattice resistance is mostly insignificant and the displacement vs time relation becomes linear. Therefore, dislocation velocities at each temperature and applied stress can be extracted from linear fits to the second half of the displacement vs time curves. Fig. 3 presents simulations of hydrogen-free cases at different temperatures and stress values, while the results for hydrogen-containing lattices can be accessed in the Supplementary Figures 24 through 26.

Fig. 4a Presents the velocity of dislocation in the hydrogen-free lattice as a function of the applied stress at different temperatures, where, in general, the velocities increase monotonically with applied stress. It can be observed from Fig. 4a that the velocity of an edge dislocation

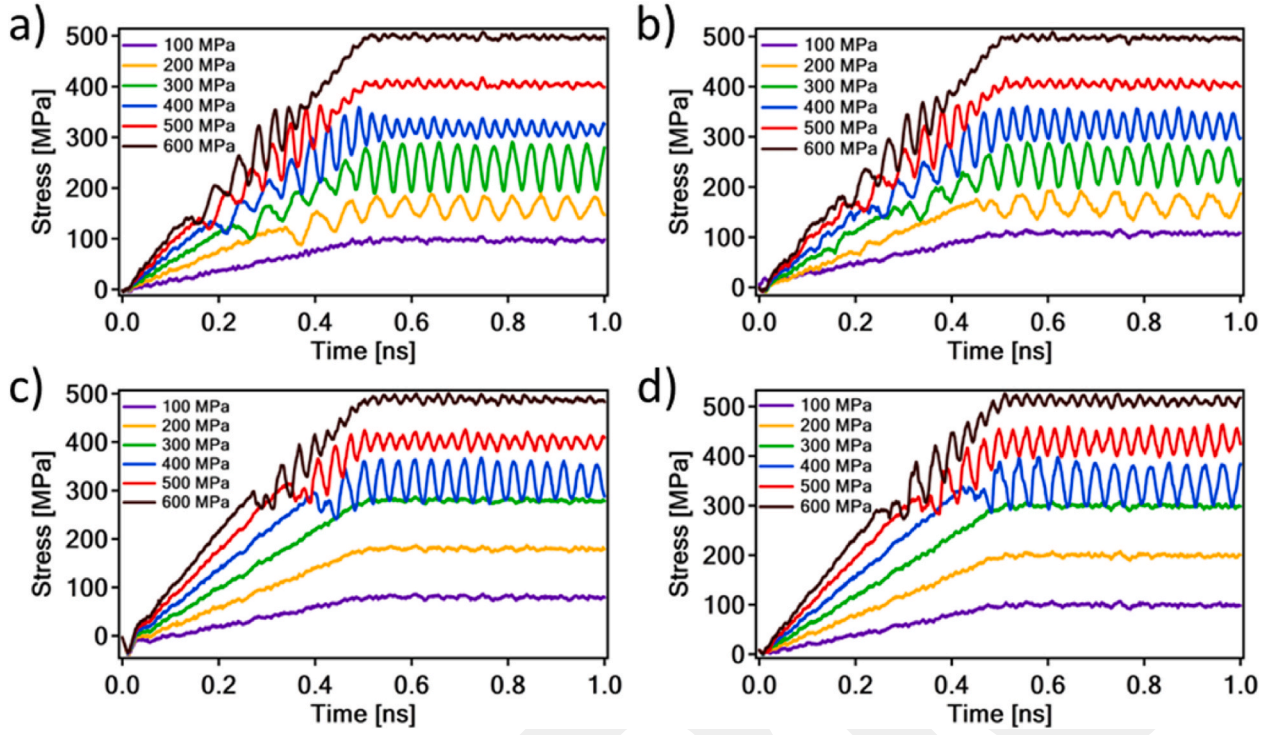

Fig. 2. Stress vs time graphs of 100 K temperature for (110) plane. Here, a) shows the pure iron case (%0 H/Fe), b) shows %0.1 H/Fe concentration, c) shows %0.25 H/Fe concentration d) shows %0.5 H/Fe concentration.

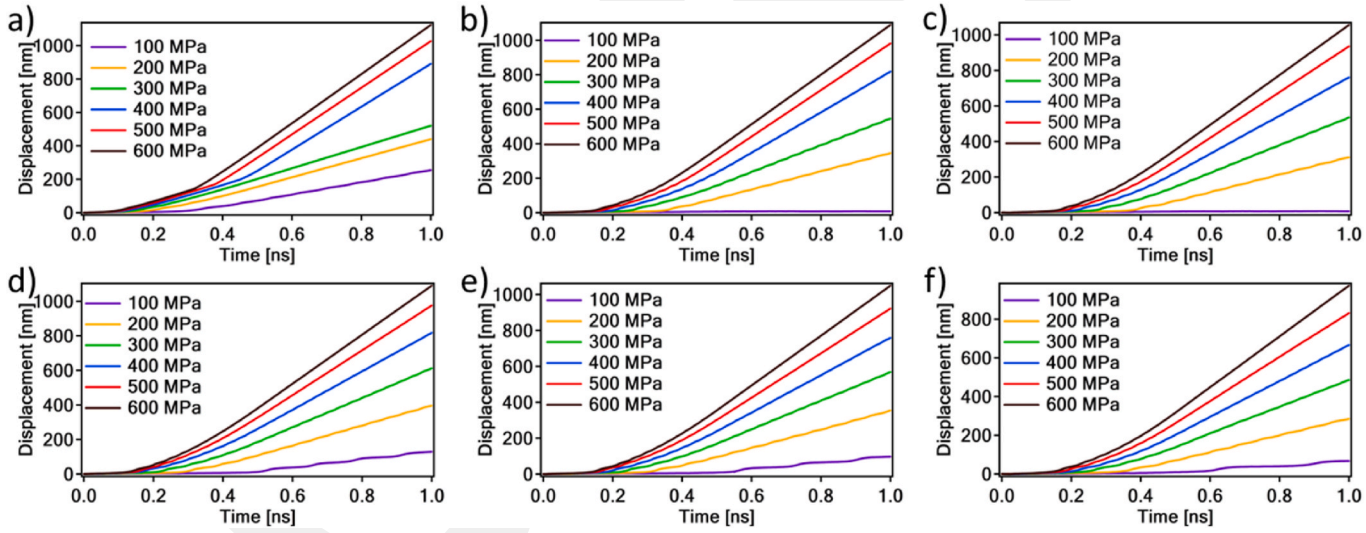

Fig. 3. Displacement vs time graphs of pure iron simulations. Here, starting from a) to f), graphs show the simulation results of 50 K, 100 K, 200 K, 300 K, 400 K, 500 K correspondingly.

increases in an approximately linear fashion with the applied stress and monotonically decreases with temperature. This behavior is attributed to phonon drag dynamics, and our results are consistent with those in the existing literature [39,58]. In particular, for a velocity of dislocation small compared to the speed of sound in a metal lattice, phonon-dislocation interactions provide a drag force that is approximately nearly proportional to the dislocation speed [38]. At higher temperatures, phonons can interact more effectively with defects such as dislocations within the crystal structure [62–64]. This increased interaction can hinder dislocation mobility, thereby decreasing overall dislocation mobility in the material [62–64]. Fig. 4b through 4f show the effect of hydrogen on the dislocation velocity in hydrogen-free and hydrogen-containing lattices at 50 K, 100 K, 200 K, 300 K and 500 K. At all temperatures, the velocity of dislocation is linearly proportional to the applied stress and the pure iron systems exhibit higher dislocation velocity values compared to the simulations with non-zero hydrogen concentration. It has been previously reported that dislocation velocity increases at higher stress values [39]. In addition, an increasing hydrogen content resulted in a lower dislocation velocity at all temperatures. Table 1 summarizes whether the dislocation is glissile (mobile) or sessile (immobile) at a given temperature and applied stress. These results clearly indicate the pinning effect of hydrogen. Specifically, if the speed of dislocation is higher than the hydrogen diffusion rate, hydrogen atoms/clusters act as a barrier to the motion of

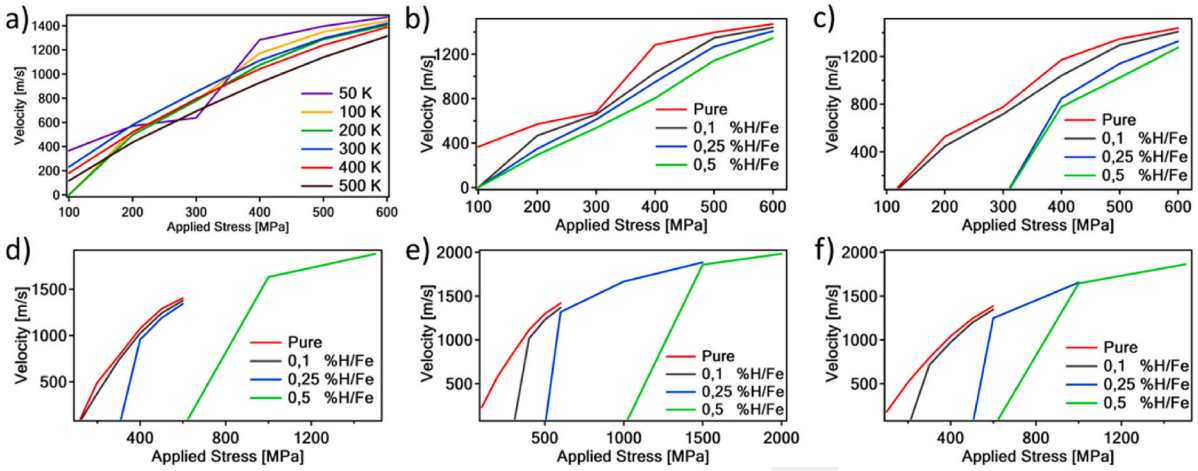

Fig. 4. Stress vs dislocation velocity graphs of a) Pure iron cell simulation results at different temperatures, b) Hydrogen-induced lattice at 50 K, c) Hydrogen-induced lattice at 100 K, d) Hydrogen-induced lattice at 200 K, e) Hydrogen-induced lattice at 300 K, f) Hydrogen-induced lattice at 400 K temperature.

Table 1
Effect of hydrogen on the dislocation mobility. g: glissile dislocation, s: sessile dislocation, N/A: Not available.

H/Fe (%)	100 MPa					200 MPa				
	50 K	100 K	200 K	300 K	400 K	50 K	100 K	200 K	300 K	400 K
0	g	s	s	g	g	g	g	g	g	g
0.1	s	s	s	s	s	g	g	g	s	s
0.25	s	s	s	s	s	g	s	s	s	s
0.5	s	s	s	s	s	g	s	s	s	s
H/Fe (%)	**300 MPa**					**400 MPa**				
	50 K	**100 K**	**200 K**	**300 K**	**400 K**	**50 K**	**100 K**	**200 K**	**300 K**	**400 K**
0	g	g	g	g	g	g	g	g	g	g
0.1	g	g	g	s	g	g	g	g	g	g
0.25	g	s	s	s	s	g	g	g	s	s
0.5	g	s	s	s	s	g	g	s	s	s

dislocation and decrease its mobility [65]. If the speed of dislocation is comparable to the hydrogen diffusion rate, hydrogen atoms/clusters can be swept at the core of the dislocation [65]. During this synchronized motion of dislocation with hydrogen, hydrogen can shield the stress field of dislocation and increase its mobility (HELP mechanism). For the transition speeds, one can observe the pinning of the dislocation by hydrogen, depinning and being caught up by hydrogen again [65]. In our simulations, the speed of dislocation is always greater than the hydrogen diffusion rate; therefore, the pinning effect of hydrogen was observed, and our results correspond well with the literature [20,34,66]. Even at higher temperatures, the effect of hydrogen on the dislocation mobility is dominant. For instance, the dislocation motion could be activated at 200 MPa for all hydrogen concentrations at 50 K, while 300 MPa, 600 MPa and 1000 MPa were required to activate the edge dislocation core at 400 K for 0.1% H/Fe, 0.25% H/Fe and 0.5% H/Fe hydrogen concentrations, respectively. Therefore, increasing both the hydrogen concentration and the temperature increases the critical stress level required to mobilize the edge dislocation core for a motion.

In the literature, for the hydrogen-free lattice, the dislocation velocity as a function of applied and critical stress, drag coefficient and burgers vector is typically written as Eq. (1), denoted as the mobility law [39]. In eq. (1), v is the dislocation velocity, τ is the resolved shear stress, that is the difference between applied shear stress and critical stress ($\tau = \tau_{app} - \tau_{critical}(T,c)$), b is burgers vector and B(T) is the drag coefficient, where T is the temperature and c is the hydrogen concentration [38]. Critical stress is the very first stress that activates the dislocation motion. For a hydrogen-free lattice, the lattice resistance for an edge dislocation is very low and the applied stress can be regarded as the resolved stress consistent with a phonon drag mechanism. Therefore, the mobility law for a hydrogen-free lattice has been formulated using $B(T) = B_0 + B_1 T$ in the equation. According to our pure α-iron simulation results, B_0 is 10^{-4} [Pa × s] and B_1 is 4×10^{-9} [Pa × s/K]. These constants are quite close to the values that are reported by G. Po et al. [38] who determined B_0 as 4.26×10^{-4} [Pa × s] and B_1 as 8.7×10^{-7} [Pa × s/K] and S. Queyreau et al. where B(T) value was determined as 6.7×10^{-7}*T [Pa × s] [39].

$$v = \frac{\tau b}{B(T)} \tag{1}$$

In the current study, the drag coefficient depends on both temperature and the hydrogen content and the resolved stress is not equal to the applied stress for the lattice containing hydrogen, and mobility law was formulated using Eq. (2) and Eq. (3) below. Critical stresses were determined from stress-time responses for all conditions and the drag coefficients of hydrogen-induced lattices were calculated by dividing the difference between applied stress and critical stress by the dislocation velocity (Fig. 4) by means of Eq. (3) for all hydrogen concentrations at different temperatures. Supplementary Fig. 27 represent the relationship of difference between applied and critical stress and velocity of dislocation at different temperatures. These figures were used to derive drag coefficients for hydrogen-induced lattices. The results are given on a logarithmic scale.

Fig. 5a shows the relationship between temperature and the drag coefficient at different hydrogen concentration values. The drag coefficient increases with both temperature and hydrogen concentration. Since there is an approximately linear relationship, the hydrogen and temperature dependent drag coefficient can be formulated as Eq. (2) and

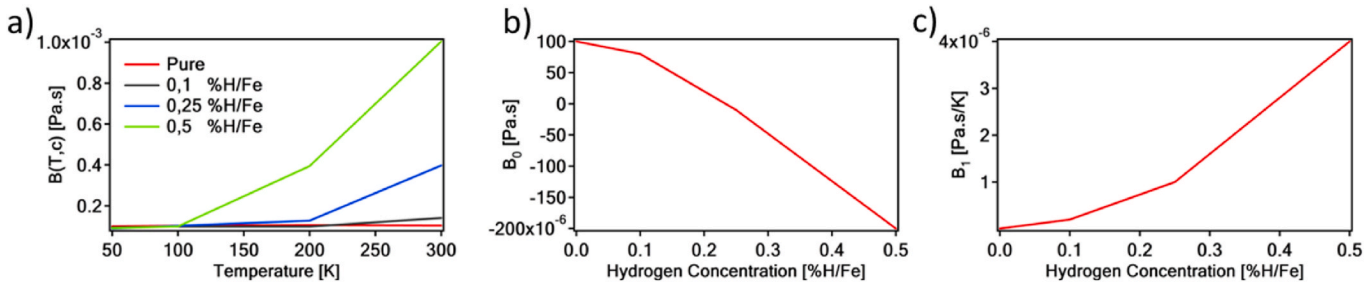

Fig. 5. Temperature vs Drag coefficient change.

the phenomenological hydrogen induced dislocation mobility of an edge dislocation can be formulated as Eq. (3):

$$B(T,c) = B_0(c) + B_1(c) * T \tag{2}$$

$$v = \frac{(\tau_{app} - \tau_{critical}(T,c))b}{B(T,c)} \tag{3}$$

Fig. 5b and c shows hydrogen concentration vs B_0 and hydrogen concentration vs B_1 graphs, respectively. They are also linearly proportional with one another via straight line. Therefore, $B_0(c)$ and $B_1(c)$ can be expressed for low hydrogen concentrations as:

$$B_0(c) = B_2 * c + B_3 \tag{4}$$

$$B_1(c) = B_4 * c + B_5 \tag{5}$$

Here, the values for B_2–B_5 were calculated from linear fits to the plots in Fig. 5b and c and are listed in Table 2. The drag coefficient of the hydrogen-containing lattice can be found for any hydrogen concentration and any temperature using these parameters (Table 2) and equations (Eqs. (2), (4) and (5)).

In order to complete the phenomenological description of the hydrogen induced dislocation mobility of an edge dislocation the dependence of the critical stress as function of hydrogen concentration and temperature should also be investigated and cast into a simple analytical expression. Fig. 6a shows the change of the critical stress values according to the given hydrogen concentrations. The critical stress, that activates the dislocation motion, increases monotonically with both temperature and hydrogen concentration. As there is a roughly linear relationship between these two (Fig. 6a), the hydrogen and temperature dependent drag coefficient can be described to a first approximation according to Eq. (6).

$$\tau_{critical}(T,c) = A_0(T) + A_1(T) * c \tag{6}$$

Fig. 6b presents the dependence of A_0, the critical shear stress at zero hydrogen concentration, on temperature. The change in A_0 is clearly not monotonic with respect to the employed temperature; therefore, it was considered constant in the temperature interval from 50 K to 400 K, where we computed the average value of A_0(T) within for all temperatures and assigned this value to be the constant value A_0 in equation (6), given in Table 2. Fig. 6c presents the dependence of A_1, the slope of hydrogen concentration – critical stress response, on temperature. Again, the increase with temperature is not monotonic, but shows a roughly overall increase. For the purpose of equation (6), A_1 was assumed to change linearly with the given temperature values and thus was essentially interpolated using Eq. (7). From the linear fit to Fig. 6c–A2, the slope of the fit, and A3, the constant of the equation, were extracted and are given in Table 2.

$$A_1(T) = A_2 * T + A_3 \tag{7}$$

Table 2 provides all the values necessary to determine the phenomenological hydrogen-induced ½<111>{110} edge dislocation mobility law.

Table 2
A and B values for the dislocation mobility of {110} glide plane.

B_2 [Pa × s/(%H/Fe)]	B_3 [Pa × s]	B_4 [Pa × s/(K*%H/Fe)]	B_5 [Pa × s/K]	A_0 [MPa]	A_2 [MPa/(K*%H/Fe)]	A_3 [MPa/%H/Fe]
$-6*10^{-4}$	1×10^{-4}	8×10^{-6}	$-4*10^{-7}$	48,97	3,8483	420,91

3.2. Edge dislocation mobility on (112) plane

Fig. 7 shows the time versus stress graph of the edge dislocation on the (112) plane at 100 K for pure Fe and Fe with 0.1%, 0.25%, and 0.5% hydrogen concentrations. The applied stress was gradually increased from 0 MPa to the desired stress value within 0.5 ns and thereafter, a constant stress is applied to the system. According to the figure, with the presence of hydrogen and increasing hydrogen concentration, the dislocation motion initiates at higher stress values. Fluctuations in the time versus stress graphs are more pronounced when the stress is near the critical stress value, indicating a transition region. When the stress is just sufficient to induce the dislocation motion, stress fluctuations are more dominant. Conversely, when the stress is more than adequate, the fluctuations are reduced. This occurs because dislocation motion within the cell alters the cell's energy. Stress, being a form of energy applied to the system, undergoes stabilization, leading to stress fluctuations. As the stress value increases, this stabilization process occurs more quickly, resulting in a smoother process. Time versus stress graphs at other temperatures are provided in the Supplementary Figures 28 through 31.

Fig. 8 presents the dislocation core displacement versus time graph for pure hydrogen-free simulations at temperatures of 100 K, 200 K, 300 K, 400 K, and 500 K, while the results for hydrogen-containing lattices are given in Supplementary Figures 32 through 34. The lowest stress values, where the dislocation motion starts, cause core displacement fluctuations due to the stress being close to the critical stress value, similar to the observation in Fig. 7. In addition, increasing the stress resulted in a greater core displacement at all temperatures. After applying linear fits to the dislocation time versus displacement graphs after 0.5 ns, the velocities of these dislocations have been calculated, as depicted in Fig. 9.

Fig. 9a–e shows the effect of hydrogen on the dislocation velocity in hydrogen-free and hydrogen-containing lattices at different temperatures and Fig. 9f shows the comparison of {110} and {112} glide planes at 100 K. At all temperatures, the dislocation velocity increases monotonically with the applied stress. The simulation cells of pure iron exhibit higher dislocation velocities compared to those with hydrogen. In addition, increasing the hydrogen content resulted in lower dislocation velocities at all temperatures (Fig. 9a–e) since hydrogen pins the dislocation and greater amount of energy is required to overcome this barrier. Our results correspond well with those in the literature [20]. Table 3 summarizes whether the dislocation is glissile or not at a given temperature and applied stress. Similar to the dislocation simulations on {110}, hydrogen also pinned the dislocation along the {112} plane due

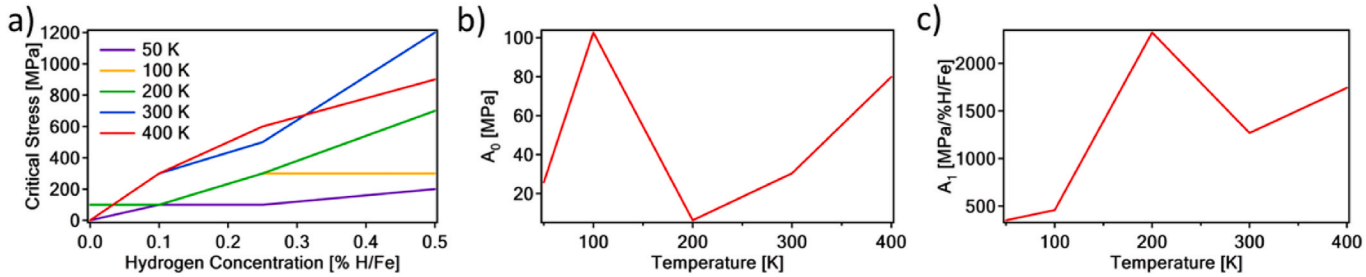

Fig. 6. Hydrogen concentration vs critical stress values for the {110} glide plane. a) presents the change of critical stress value according to the given hydrogen concentration, b) presents the change of A_0 and c) presents the change of A_1 according to the given temperature.

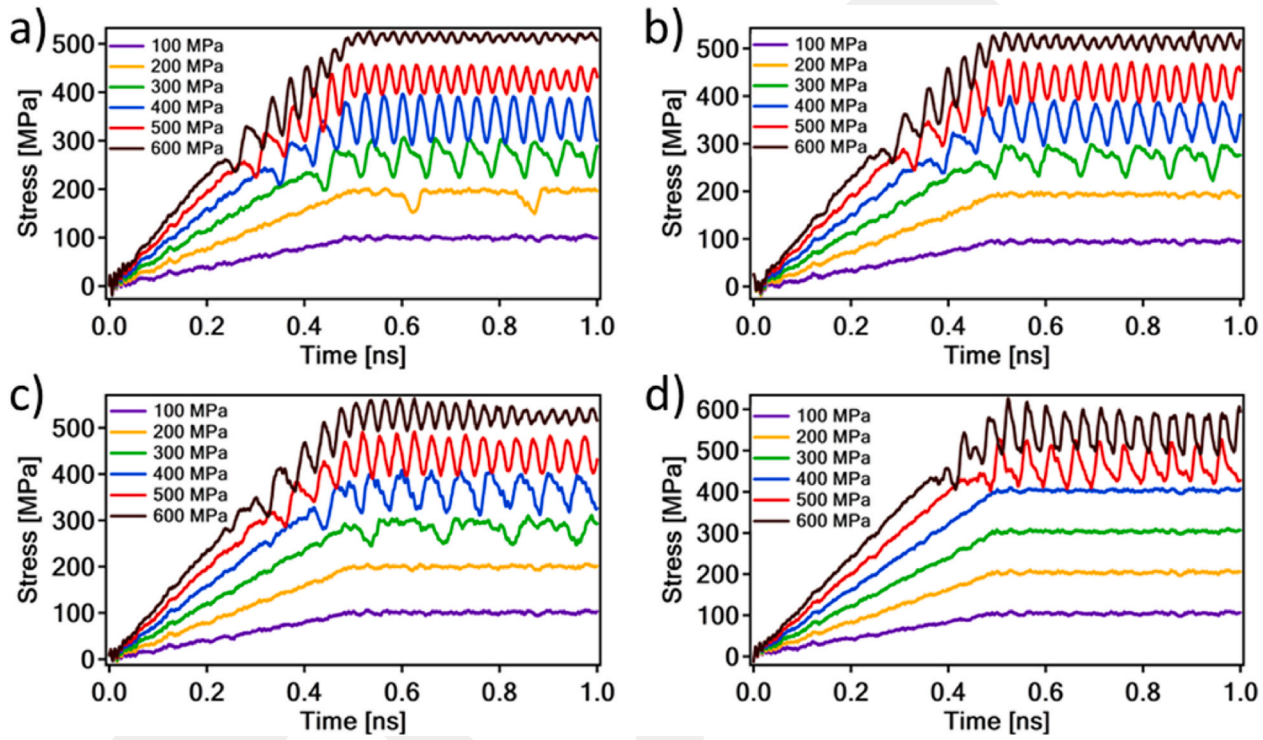

Fig. 7. Stress versus time graphs at 100 K for the {112} plane. Here, a) shows the pure iron case 0% H/Fe, b) shows 0.1% H/Fe concentration, c) shows 0.25% H/Fe concentration, and d) shows 0.5% H/Fe concentration.

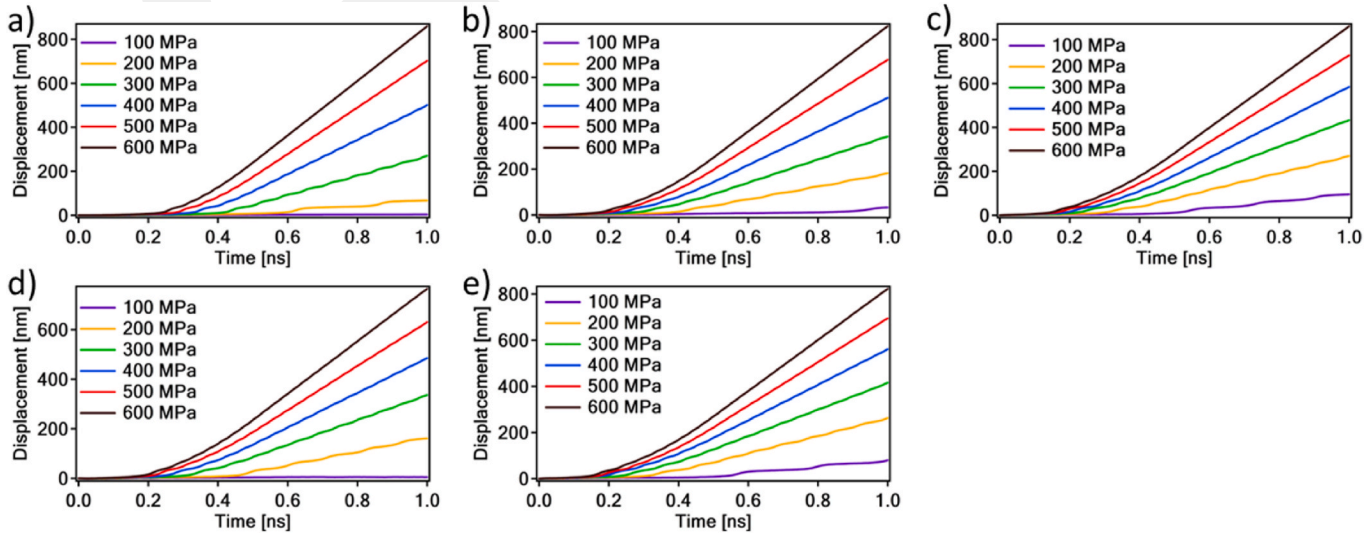

Fig. 8. Dislocation displacement vs time graph of pure iron cases. Here, from a to e, graphs belong to 100 K, 200 K, 300 K, 400 K and 500 K temperature values.

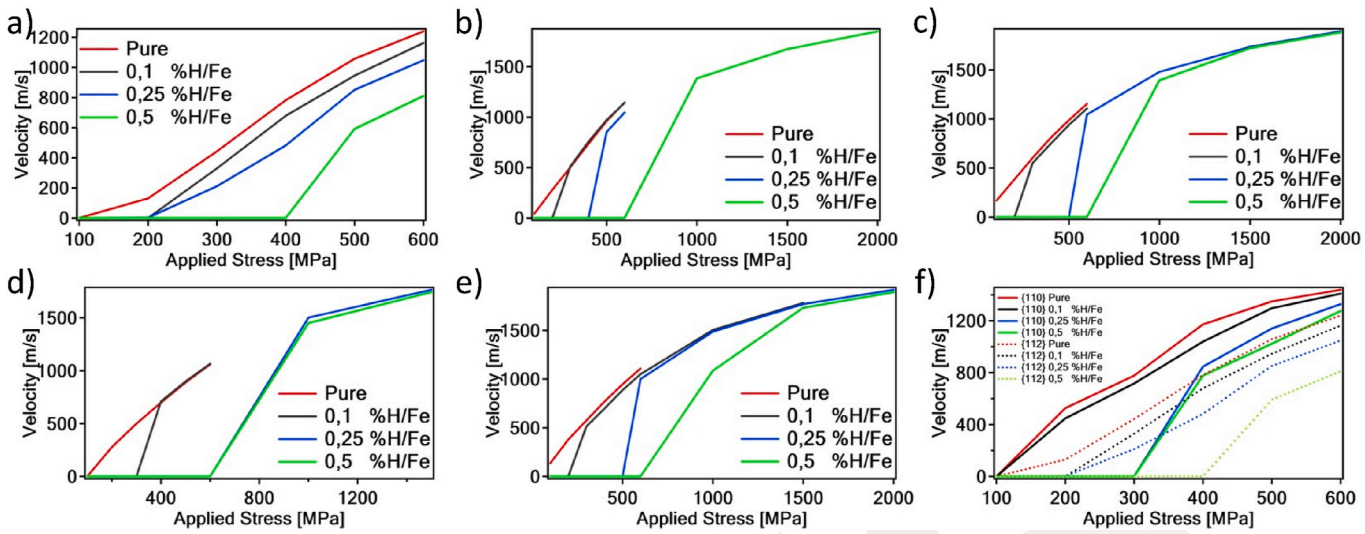

Fig. 9. Stress vs dislocation velocity graphs of a) Hydrogen-induced lattice at 100 K, b) Hydrogen-induced lattice at 200 K, c) Hydrogen-induced lattice at 300 K, d) Hydrogen-induced lattice at 400 K, e) Hydrogen-induced lattice at 500 K, f) ½ <111>{110} and ½ <111>{112} dislocations.

Table 3
Effect of hydrogen on the dislocation mobility. g: glissile dislocation, s: sessile dislocation, N/A: Not available.

H/Fe (%)	100 MPa					200 MPa				
	100 K	200 K	300 K	400 K	500 K	100 K	200 K	300 K	400 K	500 K
0	s	g	g	s	g	g	g	g	g	g
0.1	s	s	s	s	s	s	s	s	s	s
0.25	s	s	s	s	s	s	s	s	s	s
0.5	s	s	s	s	s	s	s	s	s	s

H/Fe (%)	**300 MPa**					**400 MPa**				
	100 K	**200 K**	**300 K**	**400 K**	**500 K**	**100 K**	**200 K**	**300 K**	**400 K**	**500 K**
0	g	g	g	g	g	g	g	g	g	g
0.1	g	g	g	s	g	g	g	g	g	g
0.25	g	s	s	s	s	g	s	s	s	s
0.5	s	s	s	s	s	s	s	s	s	s

to the speed of dislocation. Changing the dislocation glide plane from {110} to {112} decreases the velocity of dislocation at the same applied stress (Fig. 9f) and this result agrees well with those in the literature. It was reported that, dislocations on {110} glide planes have very low kink energies and exhibit faster kink pair formation and, furthermore, move according to the phonon drag mechanism [20]. Conversely, dislocations on {112} glide planes tend to advance through the nucleation of kink pairs in greater numbers and maintain kink formation for longer durations [20]. In addition, the ½ <111>{112} dislocation has an asymmetrical core structure, which is harder to move compared to the planar core structure. Therefore, the Peierls stress for the ½ <111>{112} dislocation is greater than the one for the ½ <111>{110} dislocation [20]. In addition, at low stress values, the motion of the ½ <111>{112} dislocation is governed by thermally activated mechanisms, while at higher stress values, viscous damping dynamics predominate, similar to the behavior observed in their ½ <111>{110} counterparts. Consequently, the glide of the dislocation {112} plane occurs significantly more slowly at low stress and temperature compared to the {110} plane. But this difference decreases at higher stress and temperature values (Fig. 9f) and this result agrees well the previous studies [20,39,40]. This result, has also been attributed to the observation that the velocity response exhibits a directional asymmetry on the {112} plane, aligning with the twinning-anti twinning (TD-AT) asymmetry [39,40]. Simulations involving hydrogen have shown that, the hydrogen environment promotes kink pair nucleation, which is more pronounced on the {112} glide plane [20].

An analytical relation for the dislocation mobility on the {112} glide plane for pure α-iron simulation can again be cast in the formula $(T) = B_0 + B_1 T$, similar to the formulation for the {110} glide plane. Here, the B_0 and B_1 values were determined as 9×10^{-5} [Pa × s] and 10^{-7} [Pa × s/K], respectively. These values were derived for hydrogen free case (c = 0) in order to compare them with literature. In the literature, the mobility law for the {112} edge dislocation has been written as $v_{(112)} = 5.5\tau_a - 1307.0$ before [39] we note this expression would also fit well with our results.

In the current study, the drag coefficient (B) depends on both temperature and the hydrogen content. To extract a mobility law from the data, the same methodology presented above for the {110} case, was followed to derive the various parameters in the equations. The change in the drag coefficient B (T,c) according to the given temperature and hydrogen concentration is presented in Fig. 10a. According to the figure, Eq. (2) can be utilized to describe the change in the drag coefficient for the {112} glide plane as well. Fig. 10b and c shows hydrogen concentration vs B_0 and hydrogen concentration vs B_1 graphs, respectively. The change in B_0 is not monotonic with respect to the hydrogen concentration (Fig. 10b); therefore, as done for the {110} plane, $B_0(T)$ was considered constant and the mean value of $B_0(T)$ was taken as a constant B_0, to use in the equations. The change in B_1 with respect to the hydrogen concentration, shown in Fig. 10c, shows a monotonic increase, and is roughly approximated by straight line, such that this dependence

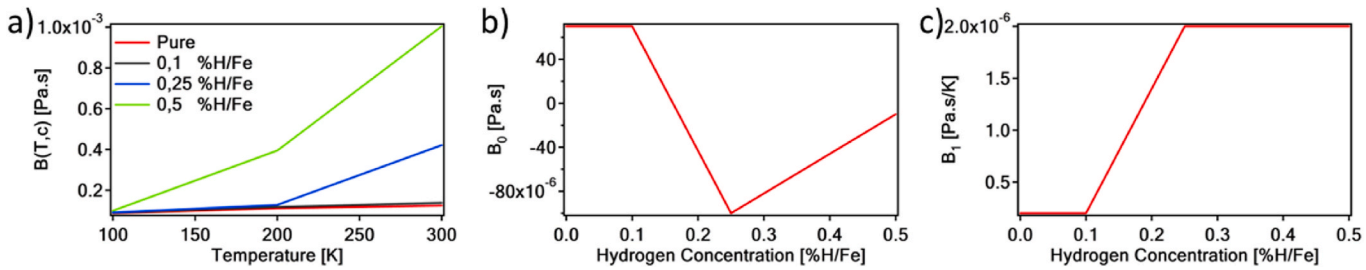

Fig. 10. Graph illustrating the change in drag coefficient with temperature for pure iron and edge dislocation on the (112) glide plane.

on hydrogen concentration can be expressed as:

$$B_1(c) = B_2 * c + B_3 \tag{8}$$

Fig. 11a shows the hydrogen concentration versus critical stress graphs for the edge dislocation on the {112} glide plane. The change in critical stress according to the given hydrogen concentration and temperature can also be formulated using Eq. (6). Here, the change in A_0 with respect to temperature is not monotonic (Fig. 11b), and thus again the mean value of A_0 is used. On the other hand, the change in A_1 with respect to temperature is roughly linear (Fig. 11c), as observed in the results for the {110} glide plane. Therefore, we perform a linear fit analogous to the one used for Eq. (7). The parameters for the description of the drag coefficients of ½ <111>{110} dislocation are given in Table 4.

According to Tables 1 and 3, on both the {110} and {112} glide planes, an analogous relationship between applied stress and dislocation mobility has been observed. This means that the dislocation mobility increases with stress. On the other hand, the dislocation mobility decreases with increasing temperature, which has been attributed to the phonon drag mechanism previously [39]. The A value, which pertains to the critical stress value calculations, is positive. This indicates that the critical stress value at which the dislocation starts to move increases with higher temperature and hydrogen concentration values.

Table 4
A and B values for the edge dislocation mobility on (112) glide plane.

B_0 [Pa × s]	B_2 [Pa × s/(K* %H/Fe)]	B_3 [Pa × s/K]	A_0 [MPa]	A_2 [MPa/(K*% H/Fe)]	A_3 [MPa]
$7,5 \times 10^{-6}$	4×10^{-6}	2×10^{-7}	63,4257	2,7387	645,34

4. Conclusion

In this study, the dependence of mobility for ½<111>{110} and ½<111>{112} edge dislocations on the presence of hydrogen was investigated and new phenomenological formulas for the analytical description of this relationship were proposed. To achieve this, molecular dynamics simulations were performed using the LAMMPS code to observe the dislocation dynamics in detail, with and without hydrogen in BCC iron, at different temperature and stress values. The following conclusions can be drawn from the study.

- Hydrogen decreases the mobility of both ½<111>{110} and ½<111>{112} edge dislocations via pinning effect.
- Kink pair formation and propagation is very fast for the edge dislocation along {110} plane so it moves with phonon drag mechanism, whereas, both thermally activated mechanisms and viscous damping dynamics constitute the motion of the ½ <111>{112} dislocation.
- Peierls stress for the ½ <111>{112} dislocation is greater than that for the ½ <111>{110} dislocation.
- Hydrogen-induced mobility laws were proposed for both ½ <111>{110} and ½ <111>{112} edge dislocations. In particular, the closed form of the hydrogen-induced mobility laws of ½<111>{110} and ½<111>{112} edge dislocations are given is Eq. (9) and Eq. (10), respectively. One can easily calculate the velocity of dislocations at any given applied stress, temperature, and hydrogen concentration. As these mobility laws are derived using four different hydrogen concentrations (0% H/Fe, 0.1% H/Fe, 0.25% H/Fe, and 0.5% H/Fe) and five different temperatures (50 K, 100 K, 200 K, 300 K, and 400 K), more accurate results are expected via interpolation. However, different mechanics and dynamics might be observed when extrapolating these values. Nonetheless, these mobility laws will still provide a very useful basis for discussion during extrapolation.

$$v_{½\langle 111\rangle\{110\}} = \frac{\left(\tau_{app} - (48{,}97 + (3{,}8483 * T + 420{,}91) * c)\right) * b}{\left(-6 * 10^{-4} * c + 1 * 10^{-4}\right) + \left(8 * 10^{-6} * c + -4 * 10^{-7}\right) * T} \tag{9}$$

$$v_{½<111>\{112\}} = \frac{\left(\tau_{app} - (63{,}4257 + (2{,}7387 * T + 645{,}34) * c)\right) * b}{7{,}5 * 10^{-6} + \left(4 * 10^{-6} * c + 2 * 10^{-7}\right) * T} \tag{10}$$

CRediT authorship contribution statement

Mehmet Furkan Baltacioglu: Writing – original draft, Formal analysis, Data curation. **Mehmet Fazil Kapci:** Methodology, Data curation. **J. Christian Schön:** Supervision, Methodology, Investigation. **Jaime Marian:** Supervision, Methodology. **Burak Bal:** Writing –

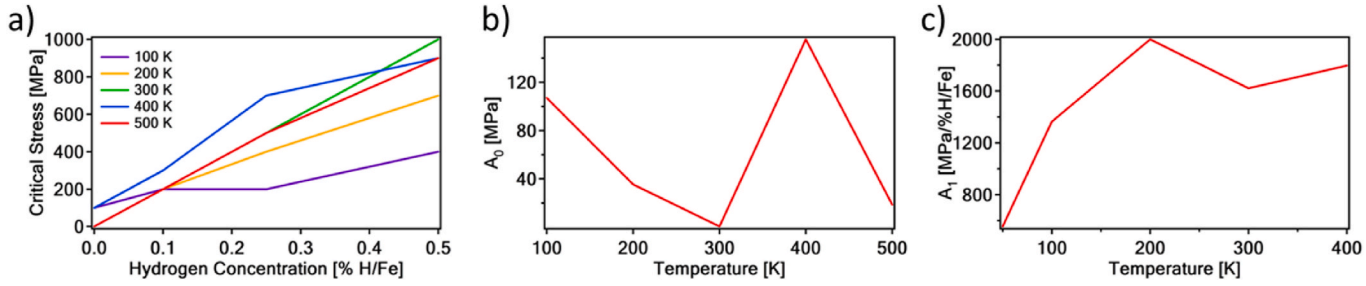

Fig. 11. A) presents the hydrogen concentration versus critical stress graphs for the (112) glide plane. b) shows the change in A_0 according to the given temperature values. c) shows the change in A_1 according to the given temperature values.

original draft, Supervision, Project administration, Methodology, Funding acquisition.

Declaration of competing interest

The authors declare the following financial interests/personal relationships which may be considered as potential competing interests:

Burak Bal reports financial support was provided by Scientific and Technological Research Council of Turkey. If there are other authors, they declare that they have no known competing financial interests or personal relationships that could have appeared to influence the work reported in this paper.

Acknowledgements

This study was supported by Scientific and Technological Research Council of Turkey (TUBITAK) under the Grant Number 122M754. The authors thank to TUBITAK for their supports.

Appendix A. Supplementary data

Supplementary data to this article can be found online at https://doi.org/10.1016/j.ijhydene.2024.08.509.

References

[1] Correa Marques S, Lima Molter D, dos S, Almeida L, Silva dos Santos D. The influence of the experimental methodology on evaluating the hydrogen embrittlement susceptibility of AISI 4340 steel manufactured by different routes. Eng Fail Anal 2024;162. https://doi.org/10.1016/j.engfailanal.2024.108361.

[2] Okonkwo PC, Barhoumi EM, Ben Belgacem I, Mansir IB, Aliyu M, Emori W, et al. A focused review of the hydrogen storage tank embrittlement mechanism process. Int J Hydrogen Energy 2023;48:12935–48. https://doi.org/10.1016/j.ijhydene.2022.12.252.

[3] Jia G, Lei M, Li M, Xu W, Li R, Lu Y, et al. Hydrogen embrittlement in hydrogen-blended natural gas transportation systems: a review. Int J Hydrogen Energy 2023;48:32137–57. https://doi.org/10.1016/j.ijhydene.2023.04.266.

[4] Lu G, Zhao Y, Zhao J, Chen Y, Long H, Li X, et al. Hydrogen embrittlement prompt fracture in Ni-based single crystal superalloy. J Mater Res Technol 2023;25:2140–51. https://doi.org/10.1016/j.jmrt.2023.06.088.

[5] Huang C, Gao X. Phase field modeling of hydrogen embrittlement. Int J Hydrogen Energy 2020;45:20053–68. https://doi.org/10.1016/j.ijhydene.2020.05.015.

[6] Shehata MF, El-Shamy AM. Hydrogen-based failure in oil and gas pipelines a review. Gas Science and Engineering 2023;115. https://doi.org/10.1016/j.jgsce.2023.204994.

[7] Venezuela J, Lim FY, Liu L, James S, Zhou Q, Knibbe R, et al. Hydrogen embrittlement of an automotive 1700 MPa martensitic advanced high-strength steel. Corrosion Sci 2020;171. https://doi.org/10.1016/j.corsci.2020.108726.

[8] Bal B, Çetin B, Bayram FC, Billur E. Effect of hydrogen on fracture locus of Fe–16Mn–0.6C–2.15Al TWIP steel. Int J Hydrogen Energy 2020;45:34227–40. https://doi.org/10.1016/J.IJHYDENE.2020.09.083.

[9] Pradhan A, Vishwakarma M, Dwivedi SK. A review: the impact of hydrogen embrittlement on the fatigue strength of high strength steel. Mater Today Proc 2020;26:3015–9. https://doi.org/10.1016/j.matpr.2020.02.627.

[10] Tuğluca IB, Koyama M, Shimomura Y, Bal B, Canadinc D, Akiyama E, et al. Lowering strain rate simultaneously enhances carbon- and hydrogen-induced mechanical degradation in an Fe-33Mn-1.1C steel. Metall Mater Trans A Phys Metall Mater Sci 2019;50:1137–41. https://doi.org/10.1007/s11661-018-5080-7.

[11] Kapci MF, Yu P, Marian J, Liu G, Shen Y, Li Y, et al. Edge dislocation depinning from hydrogen atmosphere in α-iron. Scripta Mater 2024;247. https://doi.org/10.1016/j.scriptamat.2024.116094.

[12] Dwivedi SK, Vishwakarma M. Hydrogen embrittlement in different materials: a review. Int J Hydrogen Energy 2018;43:21603–16. https://doi.org/10.1016/j.ijhydene.2018.09.201.

[13] Dwivedi SK, Vishwakarma M. Effect of hydrogen in advanced high strength steel materials. Int J Hydrogen Energy 2019;44:28007–30. https://doi.org/10.1016/j.ijhydene.2019.08.149.

[14] Xu P, Li C, Li W, Zhu M, Li W, Zhang K. Effect of microstructure on hydrogen embrittlement susceptibility in quenching-partitioning-tempering steel. Mater Sci Eng, A 2021;831:142046. https://doi.org/10.1016/j.msea.2021.142046.

[15] Tuğluca IB, Koyama M, Bal B, Canadinc D, Akiyama E, Tsuzaki K. High-concentration carbon assists plasticity-driven hydrogen embrittlement in a Fe-high Mn steel with a relatively high stacking fault energy. Mater Sci Eng 2018;717:78–84. https://doi.org/10.1016/j.msea.2018.01.087.

[16] Bal B, Okdem B, Bayram FC, Aydin M. A detailed investigation of the effect of hydrogen on the mechanical response and microstructure of Al 7075 alloy under medium strain rate impact loading. Int J Hydrogen Energy 2020;45:25509–22. https://doi.org/10.1016/j.ijhydene.2020.06.241.

[17] Najam H, Koyama M, Bal B, Akiyama E, Tsuzaki K. Strain rate and hydrogen effects on crack growth from a notch in a Fe-high-Mn steel containing 1.1 wt% solute carbon. Int J Hydrogen Energy 2020;45:1125–39. https://doi.org/10.1016/j.ijhydene.2019.10.227.

[18] Massone A, Manhard A, Drexler A, Posch C, Ecker W, Maier-Kiener V, et al. Addressing h-material interaction in fast diffusion materials—a feasibility study on a complex phase steel. Materials 2020;13:1–20. https://doi.org/10.3390/ma13204677.

[19] Baltacioglu MF, Cetin B, Bal B. The effect of strain rate on the hydrogen embrittlement susceptibility of aluminum 7075. J Eng Mater Technol 2022;145. https://doi.org/10.1115/1.4056158.

[20] Kapci MF, Schön JC, Bal B. The role of hydrogen in the edge dislocation mobility and grain boundary-dislocation interaction in α-Fe. Int J Hydrogen Energy 2021;46:32695–709. https://doi.org/10.1016/j.ijhydene.2021.07.061.

[21] Djukic MB, Bakic GM, Sijacki Zeravcic V, Sedmak A, Rajicic B. The synergistic action and interplay of hydrogen embrittlement mechanisms in steels and iron: localized plasticity and decohesion. Eng Fract Mech 2019;216. https://doi.org/10.1016/j.engfracmech.2019.106528.

[22] López Freixes M, Zhou X, Zhao H, Godin H, Peguet L, Warner T, et al. Revisiting stress-corrosion cracking and hydrogen embrittlement in 7 xxx-Al alloys at the near-atomic-scale. Nat Commun 2022;13. https://doi.org/10.1038/s41467-022-31964-3.

[23] Djukic MB, Sijacki Zeravcic V, Bakic GM, Sedmak A, Rajicic B. Hydrogen damage of steels: a case study and hydrogen embrittlement model. Eng Fail Anal 2015;58:485–98. https://doi.org/10.1016/j.engfailanal.2015.05.017.

[24] Koyama M, Tasan CC, Akiyama E, Tsuzaki K, Raabe D. Hydrogen-assisted decohesion and localized plasticity in dual-phase steel. Acta Mater 2014;70:174–87. https://doi.org/10.1016/j.actamat.2014.01.048.

[25] Popov BN, Lee JW, Djukic MB. Hydrogen permeation and hydrogen-induced cracking. In: Handbook of environmental degradation of materials. third ed. Elsevier Inc.; 2018. https://doi.org/10.1016/B978-0-323-52472-8.00007-1. 133–162.

[26] Birnbaum HK, Sofronis P. Hydrogen-enhanced localized plasticity-a mechanism for hydrogen-related fracture. Mater Sci Eng 1994;176:191–202. https://doi.org/10.1016/0921-5093(94)90975-X.

[27] Liu J, Zhao M, Rong L. Overview of hydrogen-resistant alloys for high-pressure hydrogen environment: on the hydrogen energy structural materials. Clean Energy 2023;7:99–115. https://doi.org/10.1093/ce/zkad009.

[28] Bal B, Koyama M, Gerstein G, Maier HJ, Tsuzaki K. Effect of strain rate on hydrogen embrittlement susceptibility of twinning-induced plasticity steel pre-charged with high-pressure hydrogen gas. Int J Hydrogen Energy 2016;41:15362–72. https://doi.org/10.1016/j.ijhydene.2016.06.259.

[29] Bal B, Sahin I, Uzun A, Canadinc D. A new venue toward predicting the role of hydrogen embrittlement on metallic materials. Metall Mater Trans A Phys Metall Mater Sci 2016;47:5409–22. https://doi.org/10.1007/s11661-016-3708-z.

[30] Schuler T, Christien F, Ganster P, Wolski K. Ab initio investigation of phosphorus and hydrogen co-segregation and embrittlement in α-Fe twin boundaries. Appl Surf Sci 2019;492:919–35. https://doi.org/10.1016/j.apsusc.2019.04.025.

[31] Olsson PAT, Kese K, Alvarez Holston AM. On the role of hydrogen filled vacancies on the embrittlement of zirconium: an ab initio investigation. J Nucl Mater 2015;467:311–9. https://doi.org/10.1016/j.jnucmat.2015.09.056.

[32] McEniry EJ, Hickel T, Neugebauer J. Ab initio simulation of hydrogen-induced decohesion in cementite-containing microstructures. Acta Mater 2018;150:53–8. https://doi.org/10.1016/j.actamat.2018.03.005.

[33] Tuli V, Claisse A, Burr PA. Hydrogen solubility in Zr–Nb alloys. Scripta Mater 2022;214. https://doi.org/10.1016/j.scriptamat.2022.114652.

[34] Song J, Curtin WA. Mechanisms of hydrogen-enhanced localized plasticity: an atomistic study using α-Fe as a model system. Acta Mater 2014;68:61–9. https://doi.org/10.1016/j.actamat.2014.01.008.

[35] Bhatia MA, Groh S, Solanki KN. Atomic-scale investigation of point defects and hydrogen-solute atmospheres on the edge dislocation mobility in alpha iron. J Appl Phys 2014;116. https://doi.org/10.1063/1.4892630.

[36] Itakura M, Kaburaki H, Yamaguchi M, Okita T. The effect of hydrogen atoms on the screw dislocation mobility in bcc iron: a first-principles study. Acta Mater 2013;61:6857–67. https://doi.org/10.1016/j.actamat.2013.07.064.

[37] Weinberger CR, Boyce BL, Battaile CC. Slip planes in bcc transition metals. Int Mater Rev 2013;58:296–314. https://doi.org/10.1179/1743280412Y.0000000015.

[38] Po G, Cui Y, Rivera D, Cereceda D, Swinburne TD, Marian J, et al. A phenomenological dislocation mobility law for bcc metals. Acta Mater 2016;119:123–35. https://doi.org/10.1016/j.actamat.2016.08.016.

[39] Queyreau S, Marian J, Gilbert MR, Wirth BD. Edge dislocation mobilities in bcc Fe obtained by molecular dynamics. Phys Rev B Condens Matter 2011;84. https://doi.org/10.1103/PhysRevB.84.064106.

[40] Monnet G, Terentyev D. Structure and mobility of the frac(1, 2) < 1 1 1 > {1 1 2} edge dislocation in BCC iron studied by molecular dynamics. Acta Mater 2009;57:1416–26. https://doi.org/10.1016/j.actamat.2008.11.030.

[41] Osetsky Yu N, Bacon DJ. An atomic-level model for studying the dynamics of edge dislocations in metals. Model Simulat Mater Sci Eng 2003;11:427. https://doi.org/10.1088/0965-0393/11/4/302.

[42] Gu Y, El-Awady JA. Quantifying the effect of hydrogen on dislocation dynamics: a three-dimensional discrete dislocation dynamics framework. J Mech Phys Solid 2018;112:491–507. https://doi.org/10.1016/j.jmps.2018.01.006.

[43] Yu H, Cocks A, Tarleton E. Discrete dislocation plasticity HELPs understand hydrogen effects in bcc materials. J Mech Phys Solid 2019;123:41–60. https://doi.org/10.1016/j.jmps.2018.08.020.

[44] Wen M. A new interatomic potential describing Fe-H and H-H interactions in bcc iron. Comput Mater Sci 2021;197. https://doi.org/10.1016/j.commatsci.2021.110640.
[45] Mendelev MI, Han S, Srolovitz DJ, Ackland GJ, Sun DY, Asta M. Development of new interatomic potentials appropriate for crystalline and liquid iron. Phil Mag 2003;83:3977–94. https://doi.org/10.1080/14786430310001613264.
[46] Peng S, Zhang Y-H, li B, Wang B, Chai C, Jia S, et al. Influence of hydrogen volume/specimen surface area ratio on hydrogen embrittlement sensitivity of X52 pipeline steel. Int J Pres Ves Pip 2024;209:105217. https://doi.org/10.1016/j.ijpvp.2024.105217.
[47] Zheng D, Li J, Liu B, Yu B, Yang Y, Han D, et al. Molecular dynamics investigations into the hydrogen permeation mechanism of polyethylene pipeline material. J Mol Liq 2022;368:120773. https://doi.org/10.1016/j.molliq.2022.120773.
[48] Shen J, Shen X, Zhou J, Yue W, Zhang T. Molecular dynamics simulation of fatigue damage formation in single-crystal/polycrystalline aluminum. Mater Today Commun 2024;39:109138. https://doi.org/10.1016/j.mtcomm.2024.109138.
[49] Jiao Y, Dan W, Zhang W. Effects of hydrogen on the deformation mechanism of face-centred cubic Fe–C single crystal with nanovoid: a molecular dynamics simulation. J Alloys Compd 2021;870:159330. https://doi.org/10.1016/j.jallcom.2021.159330.
[50] Zheng D, Li J, Yu B, Yang Y, Huang Z, Zhang Y, et al. Grand canonical Monte Carlo and molecular dynamics investigation of hydrogen solubility and diffusivity in nonmetallic polyvinyl chloride, polyethylene and polyvinylidene fluoride pipes materials. Fuel 2024;362:130925. https://doi.org/10.1016/j.fuel.2024.130925.
[51] Xu TH, Zhu ZQ, Geng SF, Song HY. Molecular dynamics study of effect of hydrogen atoms on mechanical properties of α-Fe nanowires. Phys Lett 2017;381:3222–7. https://doi.org/10.1016/j.physleta.2017.08.012.
[52] Li L, Du Q, Wang Y, Xu K, Sun M, Sun J, et al. Hydrogen behavior during high-temperature plastic deformation in low-alloy steels. J Mater Process Technol 2022;302:117487. https://doi.org/10.1016/j.jmatprotec.2021.117487.
[53] Song HY, Zhang L, Xiao MX. Molecular dynamics simulation of effect of hydrogen atoms on crack propagation behavior of α-Fe. Phys Lett 2016;380:4049–56. https://doi.org/10.1016/j.physleta.2016.10.019.
[54] Wang R, Cheng L, Yin C, Lou W, Wu K. The effects of hydrogen and vacancy on the tensile deformation behavior of Σ3 symmetric tilt grain boundaries in pure fe. Int J Hydrogen Energy 2023;48:30930–48. https://doi.org/10.1016/j.ijhydene.2023.04.186.
[55] Wan L, Geng WT, Ishii A, Du J-P, Mei Q, Ishikawa N, et al. Hydrogen embrittlement controlled by reaction of dislocation with grain boundary in alpha-iron. Int J Plast 2019;112:206–19. https://doi.org/10.1016/j.ijplas.2018.08.013.
[56] Stukowski A. Visualization and analysis of atomistic simulation data with OVITO–the Open Visualization Tool. Model Simulat Mater Sci Eng 2010;18:015012. https://doi.org/10.1088/0965-0393/18/1/015012.
[57] Stukowski A, Bulatov VV, Arsenlis A. Automated identification and indexing of dislocations in crystal interfaces. Model Simulat Mater Sci Eng 2012;20:085007. https://doi.org/10.1088/0965-0393/20/8/085007.
[58] Bacon DJ, Osetsky YN, Rodney D. Chapter 88 dislocation–obstacle interactions at the atomic level. In: Hirth JP, Kubin L, editors. Dislocations in solids, vol. 15. Elsevier; 2009. p. 1–90. https://doi.org/10.1016/S1572-4859(09)01501-0.
[59] Xie W, Liu X, Chen W, Zhang H. Hydrogen hardening effect in heavily deformed single crystal α-Fe. Comput Mater Sci 2011;50:3397–402. https://doi.org/10.1016/j.commatsci.2011.06.036.
[60] Sasaki D, Kusaba Y, Koyama M. Hydrogen-assisted localized plasticity driven by dislocation pinning-depinning: finite element simulations. Int J Hydrogen Energy 2024;56:280–8. https://doi.org/10.1016/j.ijhydene.2023.12.053.
[61] Wang S, Hashimoto N, Ohnuki S. Hydrogen-induced change in core structures of {110}[111] edge and {110}[111] screw dislocations in iron. Sci Rep 2013;3. https://doi.org/10.1038/srep02760.
[62] Blaschke DN, Burakovsky L, Preston DL. On the temperature and density dependence of dislocation drag from phonon wind. J Appl Phys 2021;130. https://doi.org/10.1063/5.0054536.
[63] Kuksin AY, Yanilkin AV. Atomistic simulation of the motion of dislocations in metals under phonon drag conditions. Phys Solid State 2013;55:1010–9. https://doi.org/10.1134/S1063783413050193.
[64] Hikata A, Johnson RA, Elbaum C. Interaction of dislocations with electrons and with phonons. Phys Rev B 1970;2:4856–63. https://doi.org/10.1103/PhysRevB.2.4856.
[65] Matsumoto R, Oyinbo ST, Vijendran M, Taketomi S. Hydrogen effect on the mobility of edge dislocation in α-iron: a long-timescale molecular dynamics simulation. ISIJ Int 2022;62:2402–9. https://doi.org/10.2355/isijinternational.ISIJINT-2022-311.
[66] Hasan MS, Kapci MF, Bal B, Koyama M, Bayat H, Xu W. An atomistic study on the HELP mechanism of hydrogen embrittlement in pure metal Fe. Int J Hydrogen Energy 2024;57:60–8. https://doi.org/10.1016/j.ijhydene.2023.12.274.